ISSN 2466-2232 (Print)
ISSN 2466-2100 (Online)

Evaluation of Welding Quality using Servo-Gun Displacement Data for Field Spot Welding

서보건 위치 데이터 활용 현장 저항점용접 품질 평가에 대한 기초연구

Jaesung Kim*,†, Jooheon Park*, Sanghyeok Jeong* and Bokdeok Seo**

*AI & Mechanical System Center, Institute for Advanced Engineering, Yongin, 17180, Korea
**Body manufacturing engineering team 2, KIA motors, Hwasung, 18569, Korea

†Corresponding author : kim0961@iae.re.kr
(Received August 31, 2020 ; Revised September 21, 2020 ; Accepted October 5, 2020)

Abstract

To ensure quality of spot welds, various nondestructive testing methods are used in addition to destructive testing methods, such as tensile shear tests and metallographic examination. Specifically, ultrasonic evaluation is widely used for measuring the nugget size in resistance spot welding. This study focuses on determining the possibility of establishing a standard to evaluate the quality of resistance spot welding in real time using servo-gun displacement data. Two-, three, and four-layered materials, including galvanized steel and hot stamped steel, were used in the experiment. To obtain a welding lobe diagram, we performed resistance spot welding three times under the same conditions, and secured the servo-gun data, which change depending on the expansion and contraction of the material. The strength and fracture mode data obtained from a tensile shear test were compared with the servo-gun displacement data, and the results were analyzed. The results evidently confirmed that the displacement data of the electrode of the medium-sized C gun clearly correlated with the tensile strength data of welding. However, the displacement data of the large C gun exhibited a slightly low correlation, presumably because of a mechanical issue. Furthermore, it was predicted that the results of this study could be used for real-time welding quality evaluation with minimal additional costs.

Key Words : Spot welding, Servo gun displacement value, Welding quality evaluation, Standard pattern

1. Introduction

Various types of processes such as SPR mechanical joining or TWB laser welding are being applied as different kinds of materials including ultra-high strength steel, aluminum alloy, magnesium alloy, and composite materials are used for lightening the vehicle body; however, the welding process which is most frequently applied in the production of bodywork is still resistance spot welding. For inspecting the quality of resistance spot welded joints in the field, drive check is performed for certain spot-welded parts on the body or the nugget size is measured through full destruction. Non-destructive testing is performed using ultrasound for the parts for which destructive testing is difficult to perform. For resistance spot welding, the factors that influence the quality depending on the material and thickness of the body panel are weld current (kA), weld time (cycles/ms), and electrode force (kgf/kN); among these factors, weld current and weld time are to be set in TC used in a resistance spot welder. Electrode force used to be the major cause of weld defects as the actual electrode force could not be measured during welding when a conventional pneumatic gun is used. However, electrode force can now be controlled in real time as the pneumatic gun has been replaced with a servo gun in the field where the body is assembled, thus reducing weld defects due to electrode force[1-5] .

However, weld defects in the field still remain as the main cause of downtime during body production, and therefore, diverse inspection equipment are applied while various resistance spot welding equipment are replaced such as a medium frequency direct current

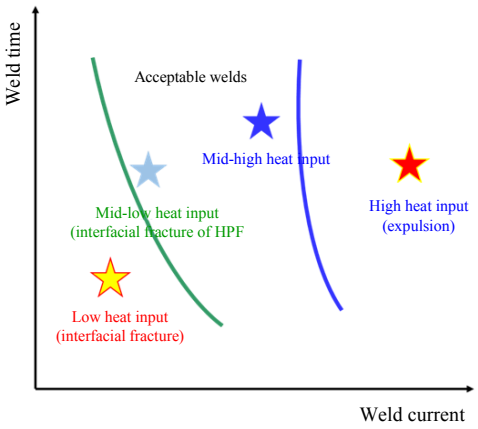

Fig. 1 Lobe graph of spot-welding quality specification in the paper

(MFDC) resistance spot welder, auto tip dresser (ATD) as well as light and color sensors.

As the application of ICT and AI has emerged across the industry in recent years, many studies are being conducted on determining the quality of resistance spot welded joints through machine learning by examining the correlation between nugget and tensile strength and the changes in electrical signal patterns such as weld current and welding voltage at the secondary side of a transformer[6-7]. Furthermore, using the parameters that can be collected at the welding system using a servo gun such as the encoder value according to the electrode displacement and motor current without requiring specific devices, a rising number of studies are being conducted on inspecting the quality of resistance spot welding through the evaluation of electrode wear characteristics and indentation depth measurement[3-4].

This study aimed to explore the possibility of establishing the criteria for assessing the resistance spot welding quality in real time using the equipment currently available in the field with the minimum costs, without applying new process or technology. Expansion and contraction occur during heating and cooling process of resistance spot welding, and these phenomena cause the changes in encoder values by inducing reactions to the electrodes controlled at an appropriate electrode force. Based on how the electrode displacement varies according to heat input, the lobe graph was divided into four sections with respect to heat input, low (low heat input, interfacial fracture), mid-low (normal heat input, button fracture), mid-high (normal heat input, button fracture), and high (excessive heat input, expulsion) as shown in Fig. 1 in order to perform welding. Then, the resistance spot welding quality was assessed based on the correlation between tensile-shear strength and servo gun displacement.

2. Experimental method

2.1 Material used

For the materials in this study, the combinations of two, three, and four panels including galvanized steel plate and hot stamping steel used for manufacturing vehicle body were selected; the type and thickness of the materials are summarized in Table 1. The chemical composition and mechanical properties of the steel used in this study are presented in Table 2 and Table 3, respectively. As shown in Fig. 2 below, the specimen used in a tensile-shear strength test was manufactured to be 100

Table 1 Material combinations for resistance spot welding

Layers	Case No.	Materials	Thickness (mm)	Total thickness (mm)
2	1	SPFC 980Y	1.2	2.6
		SPFC 590DP	1.4	
	2	SGACUD P60/P60	0.7	1.4
		SPFC 590	0.7	
3	3	SGAFC 1180 60/60	1.2	2.9
		SGACUD P60/P60	0.7	
		SGARC 440 60/60	1.0	
	4	SGACUD P60/P60	0.7	2.9
		SABC 1470 50/50	1.0	
		SPFC 590	1.2	
4	5	SGACUD P60/P60	0.7	4.9
		SGAFC 1180 60/60	1.2	
		SGAFC 590DP 60/60	1.6	
		SGAPH 440 60/60	1.4	
	6	SGAFC 1180 60/60	1.2	4.7
		SGACUD P60/P60	0.7	
		SGAFC 1180 60/60	1.2	
		SGAFC 590 DP 60/60	1.6	

Table 2 Chemical composition of materials(wt. %)

Materials	C Max.	Mn Max.	Si Max.	P Max.	S Max.
SGARC 440 60/60	0.12	1.01	0.5	0.021	0.004
SPFC 590	0.09	1.6	0.15	0.03	0.003
SPFC 590DP	0.1	2	0.2	0.03	0.003
SGAFC 590DP 60/60	0.1	2	0.2	0.03	0.003
SPFC 980 Y	0.1	2.8	1.2	0.03	0.003
SGAFC 1180 60/60	0.17	2.8	0.25	0.02	0.005
SABC 1470 50/50	0.23	1.24	0.26	0.015	0.002

Table 3 Mechanical properties of materials

Materials	0.2%YS,Mpa Spec.	TS,Mpa Spec.	El.,% Spec.
SGARC 440 60/60	270~	440~	22~
SPFC 590	350~	588~	17~
SPFC 590DP	~450	590~	24~
SGAFC 590DP 60/60	~450	590~	24~
SPFC 980 Y	580~700	980~	15~
SGAFC 1180 60/60	~850	1180~	6~
SABC 1470 50/50	950~1250	1300~1700	6~

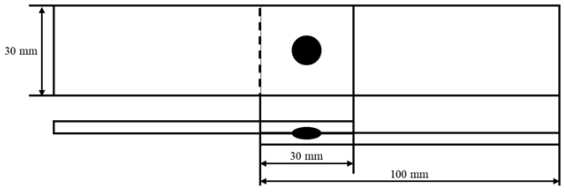

Fig. 2 Specimen for resistance spot welding

× 30 mm and the overlap length is 30 mm according to the KS B 0851 standards. For the middle plate, a 30 × 30 mm specimen was used.

2.2 Experimental equipment

The resistance spot welder used in this study is Genius MFI 408L, which is an MFDC welder, by Harms-Wende in a KSR mode which is a constant-current control method. The welding robot is a six-axis robot BX200L manufactured by Kawasaki Robotics having a nominal load capacity of 200 kg that can obtain displacement data of each axis using the data storage function, and the electrode displacement data can be obtained by attaching a servo gun. The servo guns used in the experiment are mid-size and large-size servo C-gun designed by NAWOOTEC and currently used in the field. Fig. 3 shows the guns attached to the robot. The stroke of the mid-size and large-size servo guns is 140 mm and 280 mm, respectively, and both types of servo guns used a 1.5 kW servo motor. Table 4 presents the specifications

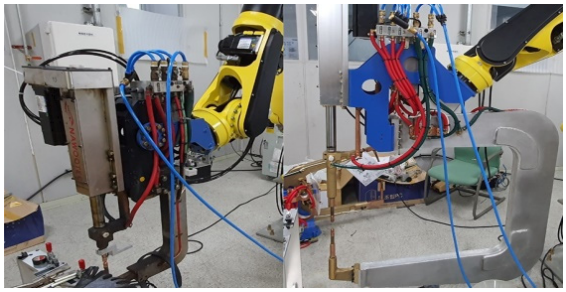

Fig. 3 Mid-size and large-size servo C-gun for resistance spot welding

Table 4 Mid-size and large-size servo C-gun specification

		Mid-size C-gun	Large-size C-gun
Motor parts	Rated output	1.5 kW	
	Rated speed	3000 r/min	
	Max. speed	4500 r/min	
	Rated torque	47.98 kgf·cm	
Moving parts	Ball screw lead	25 mm	25 mm
	Pulley Ratio	0.38	0.4
	Electrode force	500 kgf	350 kgf
	Total stroke	140 mm	280 mm
	bit resolution	11.44409	12.20703

of the servo motor. For electrodes, the Cu-Cr based composite electrodes having a diameter of 16 mm and a linear short diameter of 6 mm which are generally used for welding a vehicle body were used.

2.3 Experimental method

2.3.1 Experimental method

In the experiment, the data of servo gun displacement caused by expansion and contraction of nuggets generated during resistance spot welding of a total of six combinations of panels - two combinations of two layers, three layers, and four layers each - were collected. Exclusive jig and clamps were used for collecting only the data of servo gun displacement which is induced during welding depending on the change in the current. By setting five teaching points of the servo gun, 'home - below weld - weld - below weld - home', obtaining the noise data due to vibration during welding was minimized. The welding conditions for resistance spot welding are shown in Table 5 below. According to each panel combination, appropriate electrode force and weld time that are actually used in the field of body assembly were set. The squeeze time and cooling time were set to 200 ms and 100 ms, respectively, in order to reflect the welding conditions of the field. In order to complete a weld lobe, the weld current was increased by 0.5 kA at a time through drive check from the current at which interfacial separation occurs to the current at which expulsion occurs for welding. For securing the reproducibility of the results, welding was performed for three times at the same condition while collecting the servo gun displacement data simultaneously. Tensile-shear strength test was performed with the manufactured specimen to find the strength value, and the result was compared with the servo gun displacement data.

2.3.2 Obtaining servo gun displacement data

To examine the changes occurred due to expansion and contraction of nuggets during resistance spot welding, the start signal of welding transmitted from the robot and the servo gun displacement data are automati-

Table 5 Welding conditions for resistance spot welding

Layers	Case No.	Weld current (kA)		Force (kgf)	Weld time (ms)
		Mid-size C-gun	Large-size C-gun		
2	1	4.0~7.5	4.5~7.5	250	233
	2	4.5~8.5	4.0~8.0		
3	3	5.0~9.0	4.0~8.0		
	4	4.0~7.5	4.0~7.5	350	
4	5	5.5~8.0	5.5~9.0	300	333
	6	5.5~9.0	5.5~9.0		

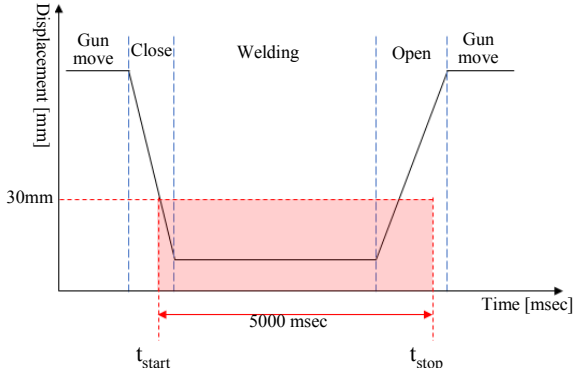

Fig. 4 Data measuring timing diagram

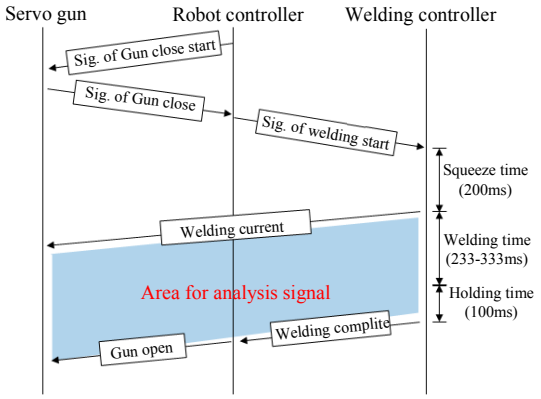

Fig. 5 Area for analysis signal

cally obtained simultaneously at the interval of 2 ms. The starting condition for acquiring the data was set to when the displacement decreases by less than 30 mm after the servo gun begins to pressurize. Data acquiring was automatically terminated when the data were collected for 5,000 ms.

2.3.3 Servo gun displacement data analysis program

The investment cost required at the body production site is minimized, and the servo gun currently used at the site is utilized to determine the welding quality at each weld spot based on the difference between the maximum and minimum displacement which is generated due to expansion and contraction of nuggets at welding section. For this purpose, a data analysis program was developed using LabVIEW manufactured by NI that can estimate accurate starting and ending sections of heat input of servo gun displacement data and calculate maximum value, minimum value, and the difference between the two extremes. The analysis areas of the servo gun data obtained thereby included the section where current actually flows and the holding time section where cooling occurs after the current stops flowing. With respect to the point at which the welding start signal generated by the robot control panel changes from 0 to 1, predetermined variables such as squeeze, welding, and holding time as well as weld current are input so as to automatically determine the analysis scope of the servo gun data. Fig. 5 shows process of obtaining data from the servo gun and the analysis area. Fig. 6 shows the GUI of the developed program and the example of the acquired data.

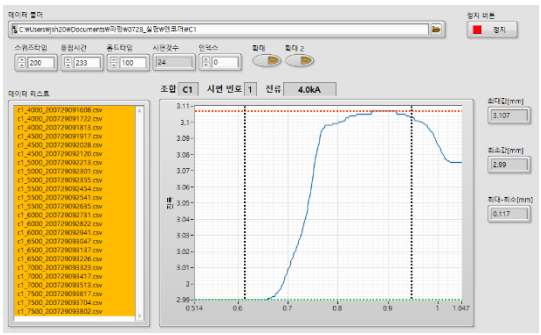

Fig. 6 Developed analysis program GUI

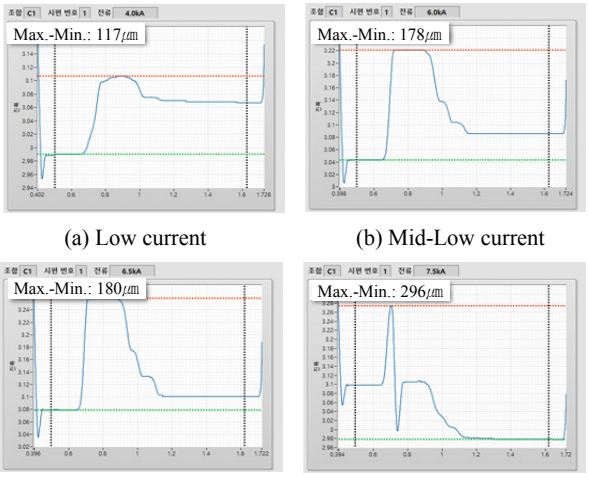

(a) Low current (b) Mid-Low current

(c) Mid-high current (d) High current

Fig. 7 Mid-size servo C-gun electrode displacement

3. Experimental results and discussion

3.1 Mid-size servo C-gun for welding

For the experiment with a mid-size servo C-gun (hereinafter, the 'mid-size gun'), the weld lobe section was divided into low heat input (interfacial separation), mid-low heat input, mid-high heat input, and high heat input (expulsion) as shown in Fig. 7. After extracting the maximum and minimum values of electrode displacement from welding start point to immediately after cooling time, during which welding is performed, from the displacement data obtained from each welding condition, the difference was used as the threshold value for determining the welding quality.

3.1.1 Mid-size servo gun displacement per current section

For the six combinations of panels (1 - 6) selected in this study, the tensile-shear strength and fracture mode according to the difference between the maximum and minimum servo gun displacement values (hereinafter, the 'servo gun displacement differential value') are shown in Figs. 9(a) - (f). The current value used for resistance spot welding is also shown. For cases 1 - 6, the servo gun displacement differential value became greater as the heat input increased in all combinations of panels. In the high heat input condition in which expulsion (spatter) occurs, the servo gun displacement data rises sharply due to instantaneous expansion which causes the servo gun displacement differential value to fluctuate significantly as shown in Fig. 7(d). For all the combinations, the difference in the displacement value between the mid-high heat input condition and expulsion condition is approximately 100 - 350 ㎛. However, in the combination 4 in which hot stamping steel is included, expulsion occurred in all lobe sections, thus confirming small changes in the servo gun displacement data depending on the difference in heat input. When the weld lobe graph was examined in terms of the fracture mode acquired from the tensile-shear test and the servo gun displacement analyzed through the welding experiment on the mid-size gun, the low heat input section below the lower limit of lobe where interfacial fracture occurs, the normal welding section, and the upper limit section where expulsion occurs could be clearly distinguished. This result contributes to the expansion of nuggets which occurs during resistance spot welding and the formation of indentation. When the weld current is applied to the specimen, thermal expansion occurs in the materials and melting occurs in the center of the electrode, followed by the expansion of a plastic zone. Subsequently, the nuggets continue to contract until the cooling time due to the electrode force applied constantly by the servo gun immediately after the maximum expansion point. Here, it is known that the nuggets are formed and the amount of displacement reduction becomes the indentation depth[8]. Therefore, the servo gun displacement related to the expansion and contraction of the material exhibits the identical pattern regardless of the panel thickness or electrode force, which has been reported as the variable reflecting the process of nugget formation. Fig. 8 shows the schematic diagram of this phenomenon. When a spatter occurs while the pressure is applied constantly by the servo motor, the servo gun displacement data rises instantly due to the increased expansion of the nugget and decreases by more than the certain displacement due to electrode force during contraction as it decreases by the volume of the separated melt.

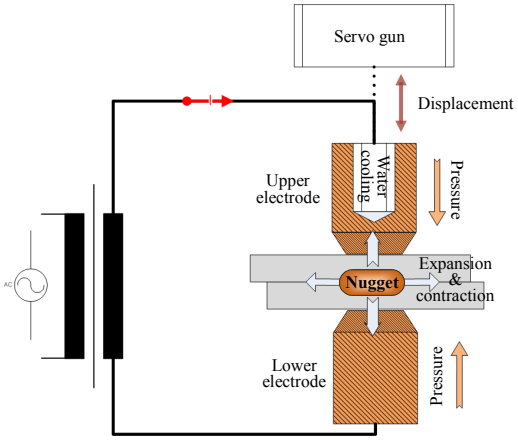

Fig. 8 Schematic diagram of servo gun displacement by nugget expansion and contraction

3.1.2 Correlation analysis between mid-size servo gun displacement and tensile-shear strength

When the encoder value of the robot controller during resistance spot welding was reviewed, the degree of expansion and contraction of the nuggets increased as the heat input increased, thus confirming the increase in the difference in the servo gun displacement values. Generally, in resistance spot welding, the nugget size becomes larger when heat input increases, and thus the welding strength increases. However, when the heat input exceeds beyond the normal level, the welding strength does not increase significantly due to the separation of the melt and internal defect of nuggets (pores) caused by expulsion. Likewise, in Figs. 9(a) - (f) which show the correlation between the servo gun displacement and tensile-shear strength, it increases linearly until the excessive heat input condition and then increases insignificantly or decreases in the excessive heat input condition. In contrast, the servo gun displacement value increases linearly from the low heat input condition to normal heat input condition, but it increases sharply in the excessive heat input condition where the servo gun expansion signal is generated significantly due to expulsion. The servo gun displacement and the tensile-shear strength increased linearly as the heat input increased; while the servo gun displacement increased sharply in the excessive heat input condition where expulsion occurred, the tensile-shear strength decreased or did not increase. Therefore, abrupt changes in the servo gun displacement values can be used as a variable for determining the normal heat input condition and excessive heat input condition during welding.

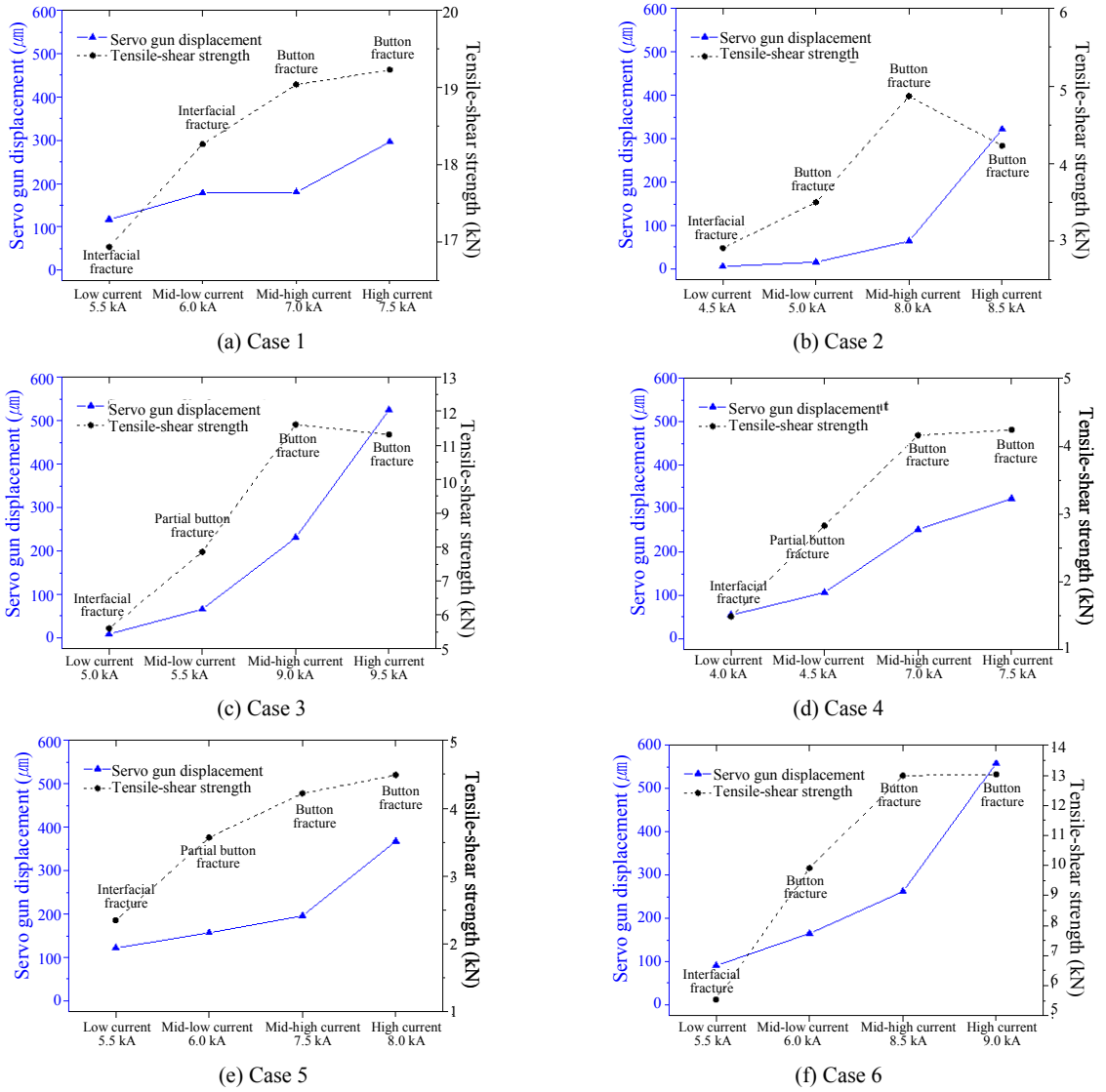

Fig. 9 Servo gun displacement, tensile-shear load and fracture mode

3.2 Large-size servo C-gun for welding

For the experiment with a large-size servo C-gun (hereinafter, the 'large-size gun'), the weld lobe section was divided into low heat input (interfacial separation), mid heat input, and high heat input (expulsion) as shown in Fig. 10 below to obtain the servo gun displacement data. Similar to the mid-size gun, the maximum and minimum values were extracted using the displacement data from the welding start point to immediately after cooling time and then the difference was examined.

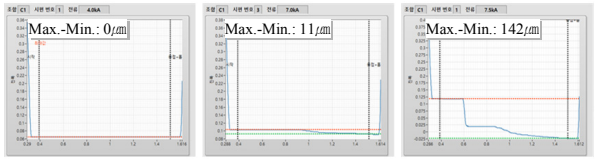

(a) Low current (b) Mid current (c) High current

Fig. 10 Large-size servo C-gun electrode displacement

3.2.1 Large-size servo gun displacement per heat input section

For the Cases 1 - 6, the servo gun displacement differential value during welding, tensile-shear strength, and fracture mode are shown in Figs. 11(a) - (f). The current value used for resistance spot welding is also shown. The servo gun displacement differential value became greater as the heat input increased in all combinations of panels. In the conditions where expulsion occurs, the servo gun displacement differential value increased as it did with the mid-size gun, but low heat input of interfacial fracture and the servo gun displacement differential value in the normal condition are

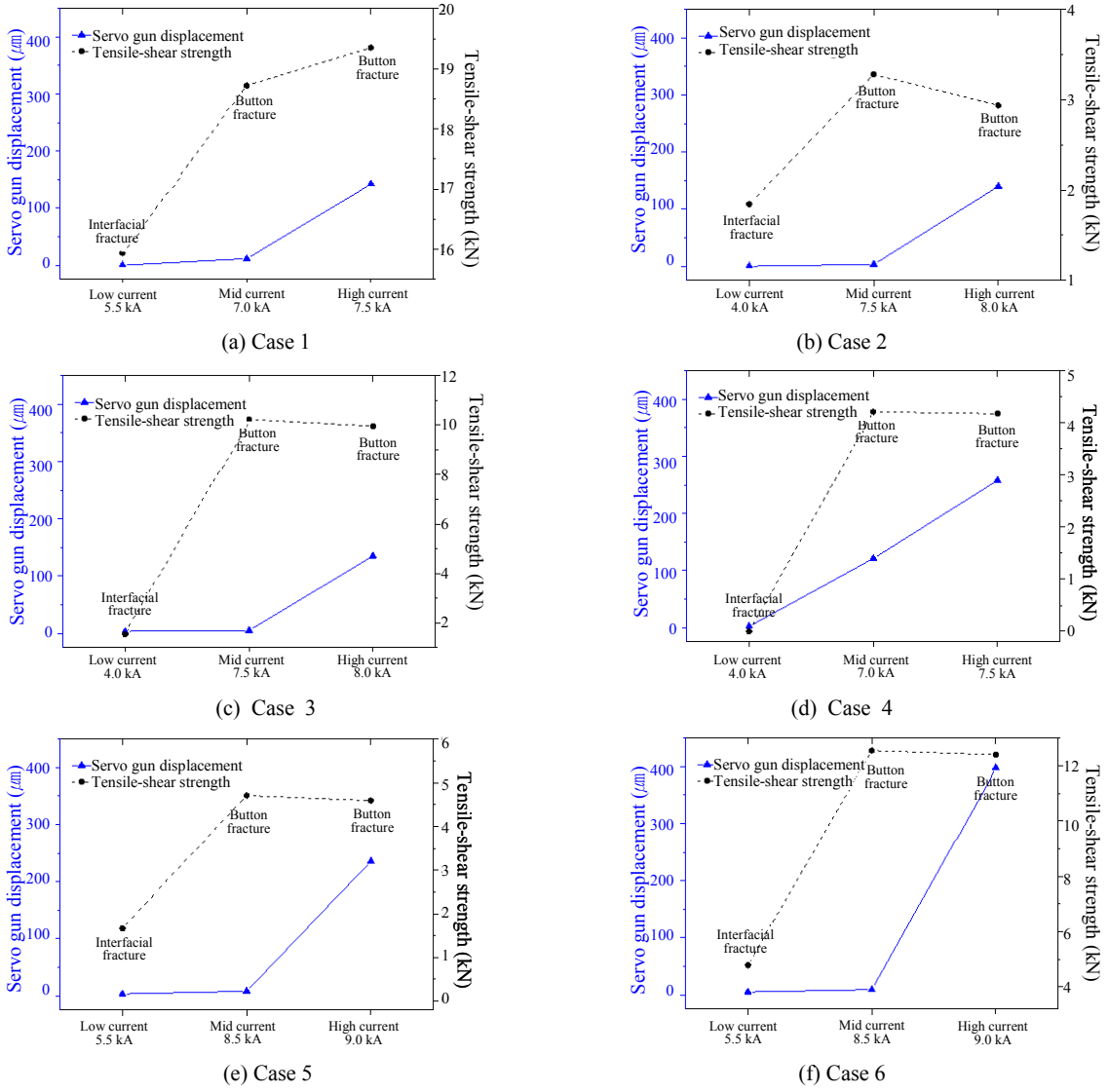

Fig. 11 Servo gun displacement, tensile-shear load and fracture mod

within several ㎛, thus causing difficulty in distinguishing the weld lobe section. It is difficult to distinguish the sections when heat input is low because the operating stroke of the large-size gun is 280 mm, which is twice as large as that of the mid-size gun, while the length of a motor rotation axis in the operating part of the upper gun is approximately 1,000 mm. When a servo gun is attached, the length of the upper apparatus part is increased, thereby partially playing a role of a damper. The entire force generated by the expansion and contraction of the material cannot be delivered to the motor encoder, thus causing the large-size gun to have a smaller displacement differential value than the mid-size gun. In the combination 4 in which hot stamping steel is included, expulsion occurred in all sections as it did with the mid-size gun, and therefore, the servo gun displacement differential value is 100 ㎛ or greater even in the normal welding condition.

Based on the results of the large-size gun, it is deemed difficult to distinguish the low heat input section below the lower limit of the weld lobe and the normal heat input section. As mentioned before, the electrode displacement value collected from the motor encoder is further reduced than the actual value due to the size of the apparatus part of the large-size gun. However, since the high heat input condition in which expulsion occurs and the normal welding condition are clearly distinguished in the weld lobe graph, welding quality of the large-size gun can also be monitored in real time.

3.2.2 Correlation analysis between large-size servo gun displacement and tensile-shear strength

The tensile-shear strength of the specimen welded with the large-size gun increased in all combinations of

panels as heat input increased as shown in Fig. 11(a) - (f), but the increase was insignificant or the strength decreased in the excessive heat input condition where expulsion occurred. Contrarily, the servo gun displacement value varied slightly from low heat input to normal heat input conditions but increased significantly in excessive heat input condition where expulsion occurred. Only in Case 4 shown in Fig. 11(d), which is the combination of panels in which hot stamping panel is included, it increased linearly from low heat input to high heat input conditions. In general, tensile-shear strength before expulsion occurs is proportional to the nugget size of resistance spot welded joints, and the degree of expansion and contraction of nuggets also increases. For the large-size gun, however, the enlarged apparatus part of the servo gun played the role of a damper for the expansion and contraction of nuggets which occurred during welding as mentioned before, which resulted in the reduction in the servo gun displacement value. Therefore, the large-size gun exhibited a significant change in the servo gun displacement value in the excessive heat input condition (expulsion) as it did with the mid-size gun; even when the tensile-shear strength increases in the low to mid heat input conditions, the long length of the apparatus part worked as a damper which caused the servo displacement value not to increase significantly.

Fig. 12 and Fig. 13 show the changes in the encoder values obtained when resistance spot welding was performed with the mid-size gun and the large-size gun, respectively. Unlike the mid-size gun, the large-size gun did not show a significant change in the servo gun displacement from when the nugget is actually expanded until the nugget formation has ended during welding. For the large-size gun, the quality difference between the low heat input and the normal heat input is difficult to distinguish, while the quality difference between the normal heat input and the excessive heat input can be clearly distinguished.

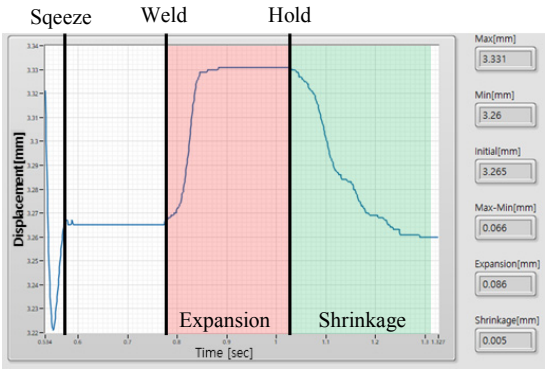

Fig. 12 Displacement of mid-size servo C-gun expansion-shrinkage (acceptable condition)

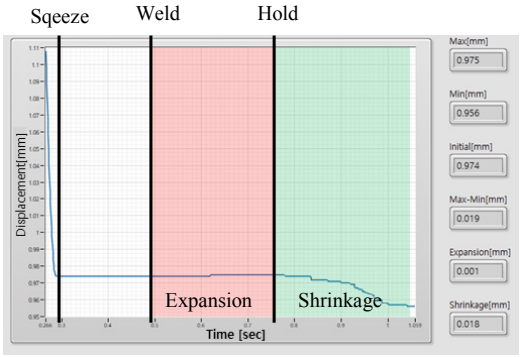

Fig. 13 Displacement of large-size servo C-gun expansion-shrinkage (acceptable condition)

4. Conclusion

In this study, the data of servo gun displacement were collected according to the expansion/contraction of the materials which occur during resistance spot welding in order to determine the welding quality at the field; the following conclusions have been reached.

1) A program was developed to calculate the servo gun displacement differential value based on the sections that have been divided into interfacial fracture, normal welding, and expulsion conditions in the resistance spot weld lobe curve.

2) For the mid-size servo C-gun, the upper limit (expulsion) and the lower limit (interfacial fracture and insufficient tensile strength) of the weld lobe curve could be clearly distinguished according to the heat input.

3) For the large-size servo C-gun, the upper limit (expulsion) and the normal condition of the weld lobe curve can be distinguished in limited cases due to the factor which is possibly attributable to the apparatus problem.

4) The technique for assessing the welding quality based on the servo gun displacement does not require additional devices and is expected to be used for determining the welding quality in real time with the minimum cost at the field.

Further studies will be conducted in the future on servo guns having varied structures to analyze how the mechanical structure of the servo gun affects the electrode displacement during resistance spot welding.

Acknowledgment

This study was supported and funded by Kia Motors/ Hyundai NGV industry-university research, the National Research Foundation of Korea (NRF-2017M3A9E2060430), the Ministry of Trade, Industry and Energy, and Korea Energy Technology Evaluation and Planning (No. 2018-1510102360).

ORCID: Jaesung Kim: https://orcid.org/0000-0002-8596-7792
ORCID: Jooheon Park: https://orcid.org/0000-0001-5991-573X
ORCID: Sanghyeok Jeong: https://orcid.org/0000-0002-9458-0792
ORCID: Bokdeok Seo: https://orcid.org/0000-0001-5134-8638

Reference

1. C. S. Lim and H. S. Chang, Spot Welding of Aluminum Alloys Using Servogun, *J. Korean Weld. Join. Soc.* 22(4) (2004) 43-49.
2. J. Y. Baek, J. G. Lee and S. H. Rhee, A Study of Dynamic Characteristic far Resistance Spot Welding Process Using Servo-gun System, *J. Korean Weld. Join. Soc.* 23(3) (2005) 40-46.
3. Y. S. Zhang, X. Y. Zhang, X. M. Lai and G. L. Chen, Online quality inspection of resistance spot welded joint based on electrode indentation using servo gun, *Sci. Technol. Weld. Join.* 12(5) (2007) 449-454. http://doi.org/10.1179/174329307x207889
4. X. Q. Zhang, G. L. Chen and Y. S. Zhang, On-line evaluation of electrode wear by servo gun in resistance spot welding, *Int. J. Adv. Manuf. Technol.* 36(7-8) (2008) 681-688. http://doi.org/10.1007/s00170-006-0885-8
5. Y. W. Park, J. G. Lee and S. H. Rhee, A Study for the Improvement of Weld Quality Through Force Control of Servo Gun in Resistance Spot Welding using Robot, *J. Korean Weld. Join. Soc.* 24(6) (2006) 13-20.
6. S. G. Choi, I. S. Hwang, M. J. Kang and S. K. Hyun, Optimization of welding parameters in resistance spot welding of 980 MPa grade GA steel sheet using multi-response surface methodology, *J. Weld. Join.* 36(4) (2018) 63-69. http://doi.org/10.5781/jwj.2018.36.4.7
7. T. H. Kim, J. Y. Yu, S. H. Rhee and Y. W. Park, Development of Intelligent Monitoring System for Welding Process Faults Detection in Auto Body Assembly, *J. Korean Weld. Join. Soc.* 28(4) (2010) 81-86. http://doi.org/10.5781/kwjs.2010.28.4.081
8. H. S. Chang and J. Y. Lee, Monitoring of Resistance Spot Welding Processes, *J. Korean Weld. Join. Soc.* 30(1) (2012) 19-26. http://doi.org/10.5781/kwjs.2012.30.1.19

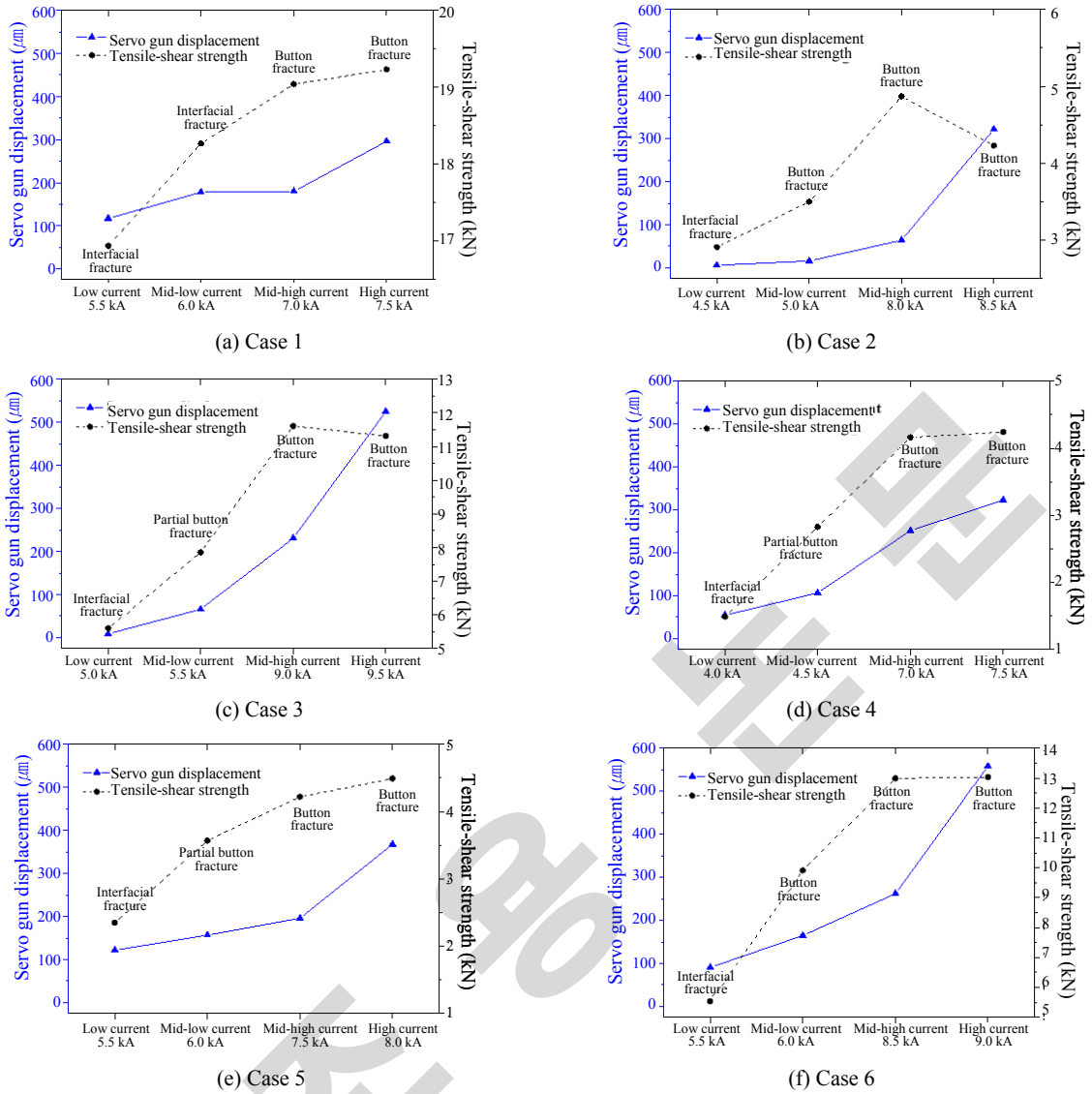

Fig. 9 Servo gun displacement, tensile-shear load and fracture mode

3.1.2 중형 서보건 Displacement와 인장전단강도의 상관관계 분석

저항점 용접시 로봇 제어기의 엔코더값을 확인한 결과 입열량이 증가할수록 너겟의 팽창과 수축이 증가하여 서보건 Displacement 값의 차이가 증가하는 것을 확인할 수 있었다. 일반적으로 저항 점용접에서는 입열량이 증가할수록 너깃의 크기가 증가하고 이에 따라 용접강도가 증가한다. 그러나 입열량이 적정 입열을 벗어나 과입열이 발생할 경우에는 날림(expulsion) 발생으로 인해 용융물의 이탈 및 너깃 내부 결함(기공) 등이 발생하므로 용접강도가 현저하게 증가하지는 않는다. 이와 마찬가지로 서보건 displacement와 전단인장강도의 관계를 보여주고 있는 Fig. 9(a)~(f)의 경우 과입열 조건 이전까지는 선형적으로 증가하다가 과입열 조건에서는 그 증가량이 미미하거나 감소하는 경향을 보이는 것을 확인할 수 있었다. 반면 서보건 displacement 값은 저입열 조건에서 적정 입열 조건까지 선형적으로 증가하는 추세를 보이나 날림이 발생하여 서보건의 팽창 신호가 크게 발생하는 과입열 조건에서는 서보건 displacement 값이 급격하게 증가함을 확인하였다. 이 결과 서보건의 displacement와 인장전단강도는 입열이 증가함에 따라 선형적으로 증가하는 것을 확인하였으며, 날림이 발생하는 과입열 조건일 때는 서보건 displacement가 급격하게 증가하는 반면 인장전단강도는 증가하지 않거나 감소하는 것을 확인하였다. 따라서 이러한 서보건 displacement 값의 급격한 변화량을 용접 중 적정입열 조건과 과입열 조건을 구분할 수 있는 변수로 사용할 수 있을 것으로 판단된다.

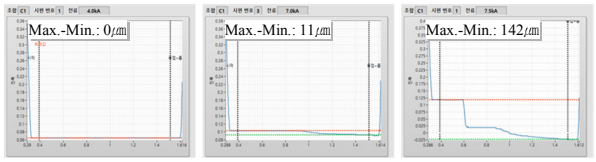

(a) Low current (b) Mid current (c) High current

Fig. 10 Large-size servo C-gun electrode displacement

3.2 대형 C형 서보 용접건

대형 C형 서보건(이하 대형건)실험에서는 용접 로브 구간을 아래 Fig. 10와 같이 저입열(계면분리), 중입열 및 고입열(날림)의 세 구간으로 분류하여 서보건 변위 데이터를 취득하였으며, 중형건과 동일하게 용접시작부터 냉각시간 직후의 변위 데이터 값을 사용하여 최대값과 최소값을 추출한 후 그 차이를 확인하였다.

3.2.1 입열 구간별 대형 서보건 Displacement

판재 조합 Case 1~6에 대해 진행한 용접 시 발생하는 서보건의 변위차이 값과 인장전단강도 및 파단모드를 Fig. 11(a)~(f)까지 그래프로 보여주고 있으며 그 때 저항 점용접에 사용된 전류 값을 표기하였다. 모든 판재 조합에서 입열량이 증가할수록 전극 변위차이 값의 크기가 증가하는 것을 확인할 수 있었다. 날림이 발생하는 조건의 경우에는 중형 C건과 마찬가지로 변위차이 값이 커지는 것을 확인하였지만, 계면 파단의 저입열과 정상조건 조건에서의 변위차이 값은 수 ㎛ 내외로 용접 로브 영역을 구분하기가 힘든 것을 확인할 수 있었다. 이처럼 입열량이 낮은 경우 영역구분이 힘든 것은 대형건의 작동 스트로크가 280 mm로 중형건과 비교하였을 때 2배 크며, 상부건 작동부의 모터 회전축으로부터의 길이는 약 1000 mm이다. 이처럼 서

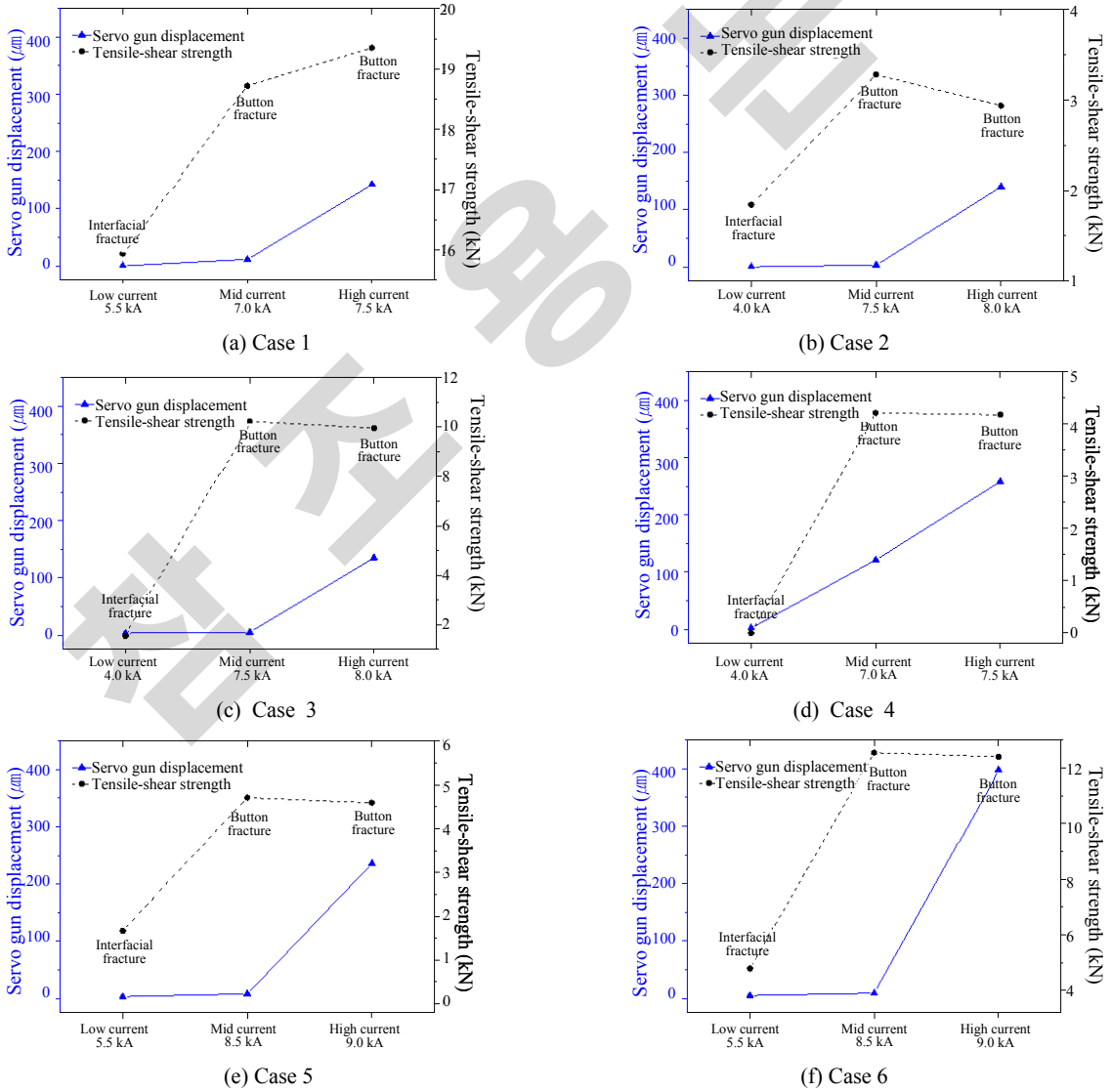

(a) Case 1 (b) Case 2

(c) Case 3 (d) Case 4

(e) Case 5 (f) Case 6

Fig. 11 Servo gun displacement, tensile-shear load and fracture mod

보건이 부착되어 있는 상부 기구부의 길이가 증가하면서 일정 부분 댐퍼 역할을 할 수 있으며, 소재의 팽창과 수축으로 발생하는 전체 힘을 모터 엔코더까지 전달하지 못하기 때문에 중형건에 비해 낮은 변위차이 값을 가지는 것으로 판단된다. 다만 핫스탬핑 강재가 포함된 조합 4의 경우 중형 C건과 유사하게 전 구간에서 날림이 발생하여 정상용접 조건에서도 변위차이 값은 100 ㎛ 이상 발생하는 것을 알 수 있었다.

대형 C건의 결과를 볼 때, 용접로브 하한선의 아래 저입열 구간과 적정 입열구간의 구분은 어려운 것으로 판단된다. 이는 앞서 언급한 것처럼 대형건의 기구부 크기로 인하여 모터 엔코더에서 수집되는 전극 변위 값이 실제보다 감소하기 때문이다. 그러나 날림이 발생하는 고입열 조건과 정상용접 조건이 용접로브 그래프 상에서 뚜렷하게 구분되므로 이를 활용하면 대형 C건의 경우에도 용접품질 판단을 위한 실시간 모니터링이 가능할 것으로 사료된다.

3.2.2 대형 서보건 Displacement와 인장전단강도의 상관관계 분석

대형 C건을 사용하여 용접한 시험편의 인장전단강도는 Fig. 11(a)~(f)의 그래프에 나타낸 것과 같이 모든 판재 조합에서 입열량이 증가함에 따라 증가하며 날림이 발생하는 과입열 조건에서는 증가량이 미미하거나 감소하는 경향을 보였다. 반면 서보건 displacement 값은 저입열에서 적정입열까지의 변화는 적었고 날림이 발생한 과입열 조건에서만 크게 증가하였다. 다만 핫스탬핑 강재가 포함된 판재 조합인 Fig. 11(d), Case 4에서만 저입열에서 고입열 조건까지 선형적으로 증가함을 확인하였다. 일반적으로 날림 발생 전의 인장전단강도는 저항 점용접부의 너깃 크기와 비례하고 너깃의 팽창과 수축의 크기도 증가한다. 그러나 대형 C형 서보건은 앞서 언급한 것과 같이 대형화 된 서보건의 기구부가 용접시 발생한 너깃의 팽창-수축에 따른 댐퍼 역

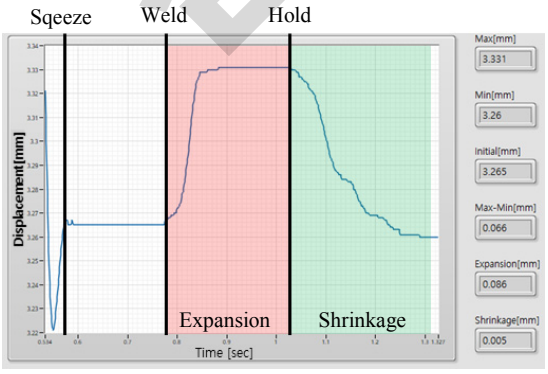

Fig. 12 Displacement of mid-size servo C-gun expansion-shrinkage (acceptable condition)

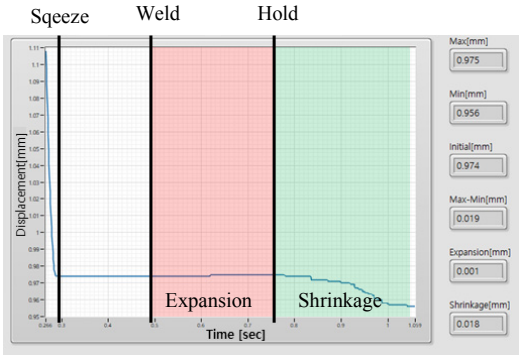

Fig. 13 Displacement of large-size servo C-gun expansion-shrinkage (acceptable condition)

할을 하였기 때문에 서보건 displacement 값이 감소한 것으로 사료된다. 따라서 대형 C건의 경우 중형 C건의 결과와 마찬가지로 과입열(날림 발생) 조건에서는 서보건 displacement 값이 크게 변화하는 경향을 보이지만, 저~중입열량 조건에서는 전단인장강도가 증가하더라도 기구부의 긴 길이가 댐퍼 역할을 하여 서보건 displacement 값의 증가량은 미비하다고 할 수 있다.

Fig. 12와 Fig. 13은 중형 C건과 대형 C건을 사용하여 저항점용접을 실시할 때 획득한 엔코더 값의 변화를 보여주고 있으며, 대형 C건의 경우 중형 C건과 달리 용접시 실제 너깃의 팽창이 발생하여 너깃 형성이 끝나는 시점까지 서보건 displacement 변화가 크게 없다는 것을 확인할 수 있다. 이처럼 대형 C건의 경우 현장에서 저입열과 적정입열에 대한 품질 구분은 어렵지만, 적정입열과 과입열에 대한 품질 상태는 명확히 구분할 수 있을 것으로 판단된다.

4. 결 론

본 논문에서는 저항 점 용접시 발생하는 소재의 팽창/수축에 따른 서보건 데이터의 변위차이 값을 수집하여 현장의 용접 품질 판단 기준으로 활용하기 위한 연구로 그에 대한 결론을 아래와 같이 서술하였다.

1) 저항점 용접의 로브 곡선에서 계면분리, 정상용접, 날림 발생 조건의 구분 기준 조건으로 사용한 서보건 데이터 변위차이 값을 계산하여 산출할 수 있는 프로그램을 개발하였다.

2) 중형 C건의 경우에는 입열량에 따라 용접 로브곡선의 상한선(날림 발생), 하한선(계면파단 및 인장강도 부족)을 명확히 구분할 수 있음을 확인하였다.

3) 대형 C건의 경우 기구적인 문제로 추정되는 요인에 의해 용접 로브곡선의 상한선(날림발생)과 정상조건을 구분할 수 있다는 다소 제한된 결론을 얻었다.

4) 서보건 전극 변위에 의한 용접 품질 판단 기법은

부가적인 장치의 추가 없이 용접 품질 판단에 사용될 수 있다는 장점이 있으며, 현장에서 최소한의 비용으로 실시간 용접 품질 판단에 활용될 수 있을 것으로 예측된다.

향후 다양한 구조의 서보건 적용한 추가적인 연구를 통해 서보건의 기계적 구조가 저항 점 용접시 발생하는 전극의 변위에 미치는 영향을 분석할 예정이다.

후 기

본 연구는 기아자동차/현대엔지비(주)의 산학연구, 한국연구재단(NRF-2017M3A9E2060430), 산업통상자원부의 재원으로 한국에너지기술평가원 (No. 20181510102-360)의 연구비 지원에 의한 연구결과임

ORCID: Jaesung Kim: https://orcid.org/0000-0002-8596-7792
ORCID: Jooheon Park: https://orcid.org/0000-0001-5991-573X
ORCID: Sanghyeok Jeong: https://orcid.org/0000-0002-9458-0792
ORCID: Bokdeok Seo: https://orcid.org/0000-0001-5134-8638

Reference

1. C. S. Lim and H. S. Chang, Spot Welding of Aluminum Alloys Using Servogun, *J. Korean Weld. Join. Soc.* 22(4) (2004) 43-49.
2. J. Y. Baek, J. G. Lee and S. H. Rhee, A Study of Dynamic Characteristic far Resistance Spot Welding Process Using Servo-gun System, *J. Korean Weld. Join. Soc.* 23(3) (2005) 40-46.
3. Y. S. Zhang, X. Y. Zhang, X. M. Lai and G. L. Chen, Online quality inspection of resistance spot welded joint based on electrode indentation using servo gun, *Sci. Technol. Weld. Join.* 12(5) (2007) 449-454. http://doi.org/10.1179/174329307x207889
4. X. Q. Zhang, G. L. Chen and Y. S. Zhang, On-line evaluation of electrode wear by servo gun in resistance spot welding, *Int. J. Adv. Manuf. Technol.* 36(7-8) (2008) 681-688. http://doi.org/10.1007/s00170-006-0885-8
5. Y. W. Park, J. G. Lee and S. H. Rhee, A Study for the Improvement of Weld Quality Through Force Control of Servo Gun in Resistance Spot Welding using Robot, *J. Korean Weld. Join. Soc.* 24(6) (2006) 13-20.
6. S. G. Choi, I. S. Hwang, M. J. Kang and S. K. Hyun, Optimization of welding parameters in resistance spot welding of 980 MPa grade GA steel sheet using multi-response surface methodology, *J. Weld. Join.* 36(4) (2018) 63-69. http://doi.org/10.5781/jwj.2018.36.4.7
7. T. H. Kim, J. Y. Yu, S. H. Rhee and Y. W. Park, Development of Intelligent Monitoring System for Welding Process Faults Detection in Auto Body Assembly, *J. Korean Weld. Join. Soc.* 28(4) (2010) 81-86. http://doi.org/10.5781/kwjs.2010.28.4.081
8. H. S. Chang and J. Y. Lee, Monitoring of Resistance Spot Welding Processes, *J. Korean Weld. Join. Soc.* 30(1) (2012) 19-26. http://doi.org/10.5781/kwjs.2012.30.1.19